Influence of coverage dependence on the thermophysical properties of adsorbates and its impact on microkinetic models

Jongyoon Bae, Bjarne Kreitz, Andrew A. Peterson*, C. Franklin Goldsmith*

School of Engineering, Brown University, Providence, Rhode Island, 02912, United States.

Abstract

This work focuses on the impact of lateral interactions on the thermophysical properties of adsorbates. We present different parameterizations for coverage-dependent enthalpy, entropy, and heat capacity in a mean-field microkinetic model. These models are tested against two systems, CO/Pt(111) and CO/Co(0001), using two different funtionals. A detailed investigation into how coverage influences the thermophysical properties of CO* is presented. Our analysis of the repulsive interaction in adsorption energy suggests that coverage effects are mainly indirect (adsorbate–metal and surface relaxation) for lower coverages, but are both indirect and direct (adsorbate–adsorbate) for higher coverages. We place a particular emphasis of studying the impact of coverage on the vibrational partition function and how this affects the entropy of adsorbates. Higher coverages typically lead to increased repulsive interactions, which should further constrain the large-amplitude modes that contribute the most to the vibrational entropy. In some cases, however, the opposite effect occurred; the vibrational entropy actually increased, because surface crowding forced adsorbates to different binding locations that had lower frequencies. However, our result highlighted cases where coverage-dependent entropy should be included, such as for adsorbates with lateral vibrational modes and for systems at high temperatures. These methods for including coverage-dependent properties into mean-field microkinetics in a thermodynamically consistent way are now available in the open-source software Cantera.

Keywords:Lateral interactions, coverage-dependent vibrational entropy, density functional theory, microkinetic modeling

1 Introduction

Catalytic reactors for industrial processes, such as Fischer-Tropsch or methanol synthesis, typically operate at high pressures, which leads to a catalyst surface covered with adsorbed reaction intermediates. Intensifying reactors for these processes or tailoring improved catalysts can be performed with multiscale modeling [1,2], which requires accurate adsorption models that capture the high-coverage phenomena. The Langmuir adsorption model for adsorbates on a solid surface is a cornerstone of contemporary modeling in heterogeneous catalysis [3]. The model assumes that a catalyst can be described as (i) a homogeneous flat surface composed of a single type of site, (ii) where no more than a single monolayer of adsorbates can form, and (iii) the adsorbates do not interact with one another – *i.e.* the adsorbed species behave ideally [3–8]. In this ideal model, an adsorbate acts merely as a site blocker against other adsorbates, and it does not otherwise influence the thermophysical properties of co-adsorbed species. Although all three assumptions are easily falsifiable, the Langmuir model is nonetheless capable of semi-quantitative adsorption/desorption behavior predictions, particularly in mean-field microkinetic (MKM) simulations.

The importance of including coverage dependence or lateral interactions was recognized early on, and a detailed survey of this history is beyond the scope of the present work. Fowler and Guggenheim pointed out in 1939 the ineffectiveness of the ideal assumption and approximated the adsorbate interaction energy as a sum of pairwise contributions among nearest neighbors [4]. The following year, Temkin [5] proposed an adsorption model, the Temkin isotherm, in which the heat of adsorption is linearly dependent on surface coverage. More recently, researchers have advanced the physicochemical understanding of the coverage effects on transition metal surfaces. Building upon pioneering work theorizing the source of lateral interactions [9–12], a series of insightful studies has led to the elucidation of physics behind the coverage effects [13–21]. The effects of coverage were observed experimentally both in adsorbate vibrational frequencies and binding energy in the form of changes in spectroscopic measurements [12, 14, 22, 23] and adsorption/desorption dynamics [14, 19, 23, 24], respectively. The lateral interactions also have been observed experimentally through infrared spectroscopy (IR), low-energy electron diffraction (LEED), temperature-programmed desorption (TPD), auger electron spectroscopy (AES), and x-ray photoelectron spectroscopy (XPS) [12, 14, 19, 23–27].

The wealth of experimental evidence confirms a significant influence of coverage on a broad range of thermophysical properties, such as adsorption energies, vibrational frequencies, binding sites, and adlayer structures. Theoretical investigations have provided insightful explanations of the origins of the coverage dependence. The compiled knowledge from theoretical work on the coverage-dependent vibrational frequency [13, 15, 28–30], binding energy [16, 18, 27, 31–37], and site preference [16, 20, 28–30] together with the experimental studies, allowed us to better understand coverage-dependent adsorption phenomenon. Furthermore, advances in computational resources combined with more sophisticated electronic structure methods have enabled a substantial improvement in the predictive power of catalytic models. Various studies have demonstrated coverage-aware kinetic models to simulate (transient) reaction processes and predict catalyst activities [31, 33–35, 37–42]. With such capabilities, the coverage-aware microkinetic models are becoming an indispensable tool for accurate prediction in heterogeneous catalysis.

In the modeling community, the vast majority of the focus has been on the enthalpic contribution to the free energy – either in terms of coverage-dependent binding energies or enthalpies of formation for adsorbates or coverage-dependent activation energies for elementary reactions [43–47].

The quantification of lateral interactions on adsorbate enthalpy range from a simpler mean-field treatment using algebraic functions [33, 34, 37, 38, 48] to a more rigorous spatially-resolved treatment using cluster expansion Hamiltonian [31, 32, 36, 38]. The effect of coverage on the entropy of an adsorbate has received far less attention, even though the coverage dependence of vibrational modes has been observed for decades [12–15, 23]. Detailed experimental information on low-frequency modes is difficult to obtain due to the detection limits, *e.g.* 200-4000 cm^{-1} for electron energy loss spectroscopy (EELS) and 1400-4000 cm^{-1} for IR [14]). Nonetheless, accurate determination of these large-amplitude, low-frequency modes is critical to the overall free energy, because these modes are responsible for the majority of the vibrational entropy. For example, the lowest vibrational mode for CO adsorbed on Pt(111) lies around $\sim 60\,\mathrm{cm}^{-1}$, corresponding to frustrated translational motions [16]. At elevated temperatures, a single harmonic oscillator with a frequency of $60\,\mathrm{cm}^{-1}$ makes a non-trivial contribution to the free energy, *e.g.* $-0.14\,\mathrm{eV}$ at $200\,^{\circ}\mathrm{C}$ and $-0.25\,\mathrm{eV}$ at $600\,^{\circ}\mathrm{C}$.

Despite the importance of lateral interactions in catalytic processes under industrial conditions, the incorporation of coverage-dependent parameters in microkinetic mechanisms remains a persistent challenge for the modeling community. Coverage dependence, if it is addressed at all, is typically included as a linear correction to the activation energy in an Arrhenius expression of an elementary rate constant, $E_a(\theta) = E_a^0 + \sum_i e_i \theta_i$, where $E_a(\theta)$ is the coverage-dependent activation energy, θ is the array of surface site fractions, E_a^0 is the activation energy in the low-coverage limit, and e_i is the "correction" to the activation energy due to the coverage of species i, which could be positive or negative [49–52]. However, arguably the single most important impact of lateral interactions is to the binding energy of adsorbates; consequently, a *kinetic* parameterization is an awkward solution to a problem that is *thermodynamic* in nature. More importantly, though, this kinetic parameterization can lead to thermodynamic inconsistency, in which the state properties enthalpy and entropy are no longer conserved [53, 54]. One aspect of this challenge is the absence of a common computational framework. CatMap, for example, includes features for coverage-dependent binding energies (and thus enthalpies of adsorption) [55]. However, it's primary focus is on the steady-state simulations of catalyst surfaces and the evaluation of rate or selectivity maps when combined with linear-scaling relationships. It is not intended to simulate reactor models or even complex networks of reactors, especially for transient systems. At present, there is no agreed-upon standard or formulation for coverage dependence in microkinetic mechanisms.

The present work addresses this gap by introducing a modeling framework for representing coverage-dependent thermophysical properties, including both enthalpy and entropy. This framework is implemented in Cantera [56], which is an open-source microkinetic modeling software package for continuum-level simulations of reactor models and reactive flow. As part of the effort to demonstrate Cantera's capabilities, a secondary aim of the present work is to evaluate the effect of coverage on the vibrational entropy of adsorbates. Two model systems of importance to many catalytic processes are used, CO adsorbed on Pt(111) (*e.g.* emission oxidation chemistry) and Co(0001) (*e.g.* Fischer-Tropsch synthesis). First, we analyze the coverage-dependent shifts in vibrational frequencies in all modes, including low-frequency modes. Our analysis provides a more complete picture of the coverage-dependent vibrational frequency shifts on top of the prior experimental investigations and how this relates to the entropy of adsorbates. Second, we compare this change in entropy to the well-established coverage effect on the enthalpy of adsorbates in mean-field microkinetic models. The combined analysis provides a holistic understanding of the impact of vibrational entropic lateral interactions against the impact of enthalpic lateral interactions.

2 Computational Methods

2.1 Electronic structure calculation

Geometry optimization, energy calculations, and vibrational analysis of CO/Pt(111) were conducted using density functional theory (DFT). The QUANTUM ESPRESSO code [57] was used in Atomic Simulation Environment (ASE) [58]. The PBE exchange-correlation functional [59] was employed and Grimme's D3 corrections [60] along with the three-body Axilrod–Teller–Muto corrections [61, 62] were applied. Plane-wave kinetic energy cutoff was 60 Ry. A periodic unit cell of 3×3 and four layers with an experimental lattice constant of 3.92 Å [63] was adopted to represent the Pt(111) surface. The bottom two layers were fixed, and a vacuum layer of 10.0 Å was applied above and underneath the Pt layers. A $(4\times4\times1)$ k-point grid was used. Model structures were optimized with a Quasi-Newton algorithm with a force convergence criteria of 0.05 eV/Å. CO* diffusion barrier energy was calculated with the dynamic nudged elastic band (dyNEB) and climbing image (CI) method [64–66], both with convergence criteria of 0.05 eV/Å.

Spin-polarized electronic structure calculations for the CO/Co(0001) system were performed with VASP [67, 68] using the BEEF-vdW [69] exchange-correlation functional. An optimized lattice constant of $a = 2.50\,\text{Å}$ and $c = 4.06\,\text{Å}$, which is in good agreement with the experimental lattice constant [63], was used for the 3×3 unit cell that was sampled with a $(5\times5\times1)$ k-point grid. The plane-wave kinetic energies were expanded to $40\,\mathrm{Ry}$, applying a first-order Methfessel-Paxton smearing with an electron temperature of $0.1\,\mathrm{eV}$.

Vibrational frequency and vibrational entropy computations were carried out with the harmonic oscillator (HO) approximation. Vibrational frequencies of CO* were calculated from a Hessian matrix using a finite-difference method [70] with a displacement magnitude of 0.01 Å via ASE. The surface atoms were fixed during the vibrational analysis, which is consistently done in the field. However, new methods are emerging that account for the impact of surface phonons on adsorption enthalpies and vibrational modes [71].

Based on the fact that CO* binds tightly, with a binding energy ($< -1.8\,\mathrm{eV}$ on Pt(111)) and a diffusion barrier greater than $k_\mathrm{B}T$ on Pt(111) (see SI), the application of HO approximation is reasonable. That said, the two lowest frequency modes, which corresponds to frustrated translation parallel to the surface (or surface diffusion), are a source of some anharmonicity. There are methods treating anharmonic modes more rigorously [72–75], but at present, those methods are designed for anharmonicity in the low-coverage limit. Incorporating coverage dependence and anharmonicity is beyond the scope of the present work, and we restrict our attention to the harmonic model, which is commonly used in the literature for CO$\cdot$.

2.2 CO adlayer configuration

The system energetics are strongly influenced by the distances between adsorbates and, thus, by the specific adsorbate arrangement on the 3×3 slab for a given coverage in 1/9$^{\text{th}}$-monolayer increments. We utilized two approaches to generate different configurations for CO on Pt(111): a simplistic configuration in which the same binding site is chosen, and a more accurate global minimum configuration. For the simplistic configuration, both atop site binding (atop-NN) and fcc hollow site binding (fcc-NN) configurations were considered. These configurations were accomplished with minimal computational effort. The first CO* was placed on a vacant site on the Pt

surface. Next, a subsequent adsorbate was placed on a nearest-neighboring (NN) site to the first adsorbate. Once all the NN sites were occupied, the next NN sites were filled. The structures were optimized after each adsorbate placement. One exception of such arrangement was made to keep all adsorbates on atop sites for atop-NN 6/9 ML, where the center adsorbate is absent to prevent any migration to other sites. Because of the well-known discrepancy between the experimentally observed CO binding site (atop site) and the DFT-calculated lowest energy binding site (fcc hollow site) [76], both sites were chosen to attain two different simplistic configuration models.

The global minimum configuration was calculated by a constrained minima hopping method [77, 78], as implemented in ASE. The method finds the global minimum structure using a combination of molecular dynamics (MD) and DFT geometry optimization [77, 79]. In the constrained minima hopping, adsorbed molecules were allowed to move and find another minimum with fictitious springs applied between adatom–surface atoms and among adsorbate atoms to prevent desorption or bond dissociation during the MD subroutine. Also, to speed up the calculations, surface atoms were fixed. The method parameters were: initial MD temperature (T_0) of 2000 K, initial acceptance energy threshold ($E_{\text{diff},\,0}$) of 2.5 eV, and spring constant of 10 eV/Å^2. The search for new minima was terminated when the MD temperature was raised above 4000 K. As a result, a collection of minima was found at each coverage, and the lowest energy configuration among the collection of minima was selected as a global minimum configuration. A final geometry optimization was performed on the lowest energy structures where the two top layers of the surface were relaxed. The adlayer configuration of CO* on Co(0001) was obtained by using the same minima hopping procedure.

2.3 Thermodynamic coverage-dependence parameterization

For a simple kinetic model with a small set of surface species, the direct computation of thermophysical properties *via* statistical mechanics methods at each time step and coverage would be tenable. However for a larger microkinetic model with multiple surface species that are relevant for technical systems, such direct thermochemistry calculations can easily accumulate computational burden. Instead, analytical forms of thermodynamic properties to reduce computational load are desired. Thus, we describe our schemes to parameterize thermodynamic coverage dependence. We have implemented a coverage-dependent thermochemistry module in Cantera. In Cantera, the user provides an input file in the YAML format (an easy, human-readable syntax for representing data) that contains the essential information: the names of the species, their thermophysical properties (typically represented as NASA polynomials, but other representations are possible), and elementary rate constants in the forward direction (typically in Arrhenius format). The reverse rate constant is computed internally assuming microscopic reversibility, $k^{\text{rev}} = k^{\text{fwd}}/K$, by first computing the free energy of reaction and thence the equilibrium constant K. This approach ensures that the mechanism is always thermodynamically consistent, even when coverage effects are included. Coverage-dependent thermophysical properties are calculated according to Equations 4–11. The coefficients in Equation 7–11 can now be included as input parameters in the mechanism YAML file, thereby enabling the evaluation of coverage-dependent thermophysical properties *via* Cantera for reactor simulations. Full details of the implementation are documented on the Cantera website (https://www.cantera.org).

Our strategy is to consider the coverage effects as a correction to the low-coverage limit. For example, the standard state enthalpy of formation at some non-zero coverage, $\Delta_{\text{f}} h^{\circ}_{\text{X}^*}(\theta_{\text{X}^*})$, is equal

to the standard state enthalpy of formation in the low-coverage limit, $\Delta_{\mathrm{f}} h^{\circ,\mathrm{ideal}}_{\mathrm{X}^*}$, plus a coverage correction term, $\Delta\Delta_{\mathrm{f}} h^{\circ,\mathrm{cov}}_{\mathrm{X}^*}(\theta_{\mathrm{X}^*})$. In our definition, a species in the low-coverage limit is identified as an ideal species (*i.e.* non-interacting). Parameters with the superscript "ideal" are the low-coverage values (here assumed to be 1/9$^{\mathrm{th}}$ monolayer (ML) coverage), and those parameters with superscript "cov" are the correction values due to the coverage dependence. Lowercase symbols are used to represent intensive properties. The corrections for the standard state (denoted with $^\circ$, evaluated at 1 bar and 298 K) enthalpy of formation and reference entropy, along with the correction for heat capacity for an arbitrary adsorbate X* are formulated in Equations 1, 2, and 3, respectively:

$$\Delta\Delta_{\mathrm{f}} h^{\circ,\mathrm{cov}}_{\mathrm{X}^*}(\theta_{\mathrm{X}^*}) \equiv \Delta_{\mathrm{f}} h^{\circ}_{\mathrm{X}^*}(\theta_{\mathrm{X}^*}) - \Delta_{\mathrm{f}} h^{\circ,\mathrm{ideal}}_{\mathrm{X}^*}(\theta_{\mathrm{X}^*} = 1/9\ \mathrm{ML}) \tag{1}$$

$$\Delta s^{\circ,\mathrm{cov}}_{\mathrm{X}^*}(\theta) \equiv s^{\circ}_{\mathrm{X}^*}(\theta_{\mathrm{X}^*}) - s^{\circ,\mathrm{ideal}}_{\mathrm{X}^*}(\theta_{\mathrm{X}^*} = 1/9\ \mathrm{ML}) \tag{2}$$

$$\Delta c^{\circ,\mathrm{cov}}_{p_{\mathrm{X}^*}}(T, \theta_{\mathrm{X}^*}) \equiv c^{\circ}_{p_{\mathrm{X}^*}}(T, \theta_{\mathrm{X}^*}) - c^{\circ,\mathrm{ideal}}_{p_{\mathrm{X}^*}}(T, \theta_{\mathrm{X}^*} = 1/9\ \mathrm{ML}) \tag{3}$$

By combining these corrections with the heat capacity, we can express the enthalpy of formation and entropy of an adsorbate at arbitrary temperatures and coverages:

$$\Delta_{\mathrm{f}} h^{\circ}_{\mathrm{X}*}(T,\theta) = \underbrace{\Delta_{\mathrm{f}} h^{\circ,\mathrm{ideal}}_{\mathrm{X}*} + \int_{298\ \mathrm{K}}^{T} c^{\circ,\mathrm{ideal}}_{p_{\mathrm{X}*}}(T)\, dT}_{\text{low-coverage limit}} + \underbrace{\Delta\Delta_{\mathrm{f}} h^{\circ,\mathrm{cov}}_{\mathrm{X}*}(\theta) + \int_{298\ \mathrm{K}}^{T} \Delta c^{\circ,\mathrm{cov}}_{p_{\mathrm{X}*}}(T,\theta)\, dT}_{\text{coverage dependence}} \tag{4}$$

$$s^{\circ}_{\mathrm{X}*}(T,\theta) = \underbrace{s^{\circ,\mathrm{ideal}}_{\mathrm{X}*} + \int_{298\ \mathrm{K}}^{T} \frac{c^{\circ,\mathrm{ideal}}_{p_{\mathrm{X}*}}(T)}{T} dT}_{\text{low-coverage limit}} + \underbrace{\Delta s^{\circ,\mathrm{cov}}_{\mathrm{X}*}(\theta) + \int_{298\ \mathrm{K}}^{T} \frac{\Delta c^{\circ,\mathrm{cov}}_{p_{\mathrm{X}*}}(T,\theta)}{T} dT}_{\text{coverage dependence}} \tag{5}$$

$$c^{\circ}_{p_{\mathrm{X}*}}(T,\theta) = c^{\circ,\mathrm{ideal}}_{p_{\mathrm{X}*}}(T) + \Delta c^{\circ,\mathrm{cov}}_{p_{\mathrm{X}*}}(T,\theta) \tag{6}$$

The coverage dependencies of enthalpy of formation, entropy, and heat capacity were parameterized from DFT-derived quantities in this work. At different coverages, zero-point energy (ZPE) corrected electronic energy and vibrational frequencies were calculated and then converted into enthalpy of formation, entropy, and heat capacity using standard statistical-mechanics models for harmonic oscillators. Enthalpies of formation were derived according to the approach outlined by Blondal et al. [80]. This approach integrates the DFT data into the global thermochemical network of the Active Thermochemical Tables (ATcT) using gas-phase CH_4, H_2, H_2O, and the vacant surface as the atomic reference basis set [81]. The calculated thermophysical quantities were referenced to those of the low-coverage limit, at 1/9th ML, to get coverage dependence parameters as described in Equations 1–3.

The results were transformed from discrete values into a continuous form using different algebraic formulas. The differences relative to the low-coverage limit for the formation enthalpy and entropy—Equations (1) and (2), respectively—were fitted with the four algebraic forms: linear, piecewise linear, polynomial, and interpolative. The exact algebraic expressions are given in Equations 7–10, where f can be either $\Delta\Delta_{\mathrm{f}}h^{\circ,\mathrm{cov}}_{\mathrm{X}^*}$ or $\Delta s^{\circ,\mathrm{cov}}_{\mathrm{X}^*}$. The first three forms have been adopted frequently by previous studies [34, 38, 55], with the linear form being used most frequently [82]. For the polynomial form, we chose a 3$^{\mathrm{rd}}$-order polynomial based on the balance between accuracy and overfitting, which was observed by extraneous curvatures when the 4$^{\mathrm{th}}$-order polynomial was used. We also employed an interpolative model that computes a value at a coverage of interest by linearly interpolating between two adjacent data points, one at coverage directly lower than and another at coverage directly greater than the coverage of interest. To the best of our knowledge, the interpolative model is employed for the first time. Because the heat capacity depends on temperature and coverage, we employed a log-quadratic expression (Equation 11). Coefficients c_1–c_8 were fitted from the DFT-derived thermodynamic parameters.

$$f^{\circ,\mathrm{cov}}_{\mathrm{X}^*}(\theta) = c_1\theta_{\mathrm{X}^*} \tag{7}$$

$$f^{\circ,\mathrm{cov}}_{\mathrm{X}^*}(\theta) = \begin{cases} c_2\theta_{\mathrm{X}^*} & , \theta_{\mathrm{X}^*} \leq \theta^{\mathrm{switch}}_{\mathrm{X}^*} \\ c_3(\theta_{\mathrm{X}^*} - \theta^{\mathrm{switch}}_{\mathrm{X}^*}) + (c_2\theta^{\mathrm{switch}}_{\mathrm{X}^*}) & , \theta_{\mathrm{X}^*} > \theta^{\mathrm{switch}}_{\mathrm{X}^*} \end{cases} \tag{8}$$

$$f^{\circ,\mathrm{cov}}_{\mathrm{X}^*}(\theta) = c_6{\theta_{\mathrm{X}^*}}^3 + c_5{\theta_{\mathrm{X}^*}}^2 + c_4\theta_{\mathrm{X}^*} \tag{9}$$

$$f^{\circ,\mathrm{cov}}_{\mathrm{X}^*}(\theta) = \frac{f^{\circ,\mathrm{cov}}_{\mathrm{X}^*}(\theta^{\mathrm{higher}}_{\mathrm{X}^*}) - f^{\circ,\mathrm{cov}}_{\mathrm{X}^*}(\theta^{\mathrm{lower}}_{\mathrm{X}^*})}{\theta^{\mathrm{higher}}_{\mathrm{X}^*} - \theta^{\mathrm{lower}}_{\mathrm{X}^*}}(\theta_{\mathrm{X}^*} - \theta^{\mathrm{lower}}_{\mathrm{X}^*}) + f^{\circ,\mathrm{cov}}_{\mathrm{X}^*}(\theta^{\mathrm{lower}}_{\mathrm{X}^*}), \quad \theta^{\mathrm{lower}}_{\mathrm{X}^*} \leq \theta_{\mathrm{X}^*} < \theta^{\mathrm{higher}}_{\mathrm{X}^*} \tag{10}$$

$$\Delta c^{\circ,\mathrm{cov}}_{p_{\mathrm{X}^*}}(T,\theta) = [c_7\ln(T) + c_8]{\theta_{\mathrm{X}^*}}^2 \tag{11}$$

These new coverage-dependent thermochemistry features in Cantera were recently used by our group for the CO_2 methanation [40], the oxidation of exhaust gas emissions from an internal combustion engine [41, 83], and the non-oxidative dehydrogenation of C_2H_6 [84]. However, only the effect of coverage on the formation enthalpy was considered in these papers. Lastly, the method is not restricted to self-interactions; rather, the user can create as many cross terms as necessary, given available data.

2.4 Microkinetic modeling

The impact of coverage dependence on the thermophysical properties of adsorbed CO on Pt(111) and Co(0001) was assessed in equilibrium calculations and in transient simulations using Cantera. For equilibrium predictions, a CO adsorption isotherm was calculated with Equation (13):

$$* + \mathrm{CO(g)} \rightleftharpoons \mathrm{CO}^* \tag{12}$$

$$\theta_{\mathrm{CO}^*} = \frac{\sqrt{K_\mathrm{p} p_{\mathrm{CO}^*}}}{1 + \sqrt{K_\mathrm{p} p_{\mathrm{CO}^*}}} \tag{13}$$

where K_p is the partial-pressure equilibrium constant, $K_\mathrm{p} = K/p^0$, K is the true equilibrium constant, and p^0 is the standard state reference pressure of 1 bar. Temperature-programmed desorption (TPD) of CO was used for the transient simulations, using a TPD model from previous work [85]. TPD simulations with the single-crystal surfaces of Pt(111) and Co(0001) were performed with a temperature ramp of $20\,\mathrm{K\,min^{-1}}$ at ultra-high vacuum condition of $1 \times 10^{-7}\,\mathrm{bar}$. The catalyst surface was initialized with a coverage of 0.6 ML at $300\,\mathrm{K}$. Parameters for the TPD simulation are taken from previous work; we assumed a catalyst surface area of $10.4\,\mathrm{m^2\,g^{-1}}$ and a catalyst mass of $0.04\,\mathrm{g}$ [85]. The catalyst was flushed with $50\,\mathrm{mL_N\,min^{-1}}$ of N_2 during the TPD.

3 Results and Discussion

3.1 Coverage dependence on the adsorption energy

The three configurations of CO* on Pt(111) obtained from the global minimum (global min) and the two simplistic models with initial atop site binding (atop-NN) and with initial fcc hollow site binding (fcc-NN) are presented in Figure 1. The configurations are in roughly equidistant arrangements, consistent with predictions from the previously reported CO* adlayer structures on transition metals [12, 14, 16, 24]. This agreement implies that our global minima model is physically sound. The global minimum adlayer model computed the lowest energy configuration for the entire range of coverages by discovering a total of 382 unique different configurations. The most stable binding site of CO from the global minima model is in the hollow site, whereas experiments show that CO favors adsorption on atop sites. This discrepancy from DFT calculations is well-known and it requires higher-level of theory calculations to predict the correct adsorption site [86].

The four sites in Pt(111) are composed of different numbers of Pt atoms: atop, bridge, fcc hollow and hcp hollow sites are 1-fold, 2-fold, 3-fold, and 3-fold sites, respectively, and they each have a unique energy of adsorption, which can vary as much as 0.12 eV (Figure S3). Sequentially, when a configuration's average n-fold value falls below 2, it implies adsorbate configurations that are primarily located on atop sites, and an average n-fold value above 2 means they are mostly on hollow sites. As can be seen in Figure 2, the atop-NN and fcc-NN models stay in the atop-site-dominant region and hollow-site-dominant region, respectively, throughout the entire range of coverage. However, there indeed is a transition from adsorbates on mostly hollow sites to mostly atop sites across $\sim$0.5 ML coverage in the global minimum model. Previously, it was reported that the preferred adsorbate arrangements at different coverages entailed site-to-site conversion, which results in mixed-site occupation [16, 20, 24, 29, 30]. The phenomenon has been explained by combinatory effects from a balancing between inherent, low-coverage site preference and keeping the furthest distance from each other to minimize through-space repulsion [20]. Another explanation of the phenomena is provided by attractive dipolar interactions among opposite-signed atop site bound adsorbates and bridge/hollow site bound adsorbates [30].

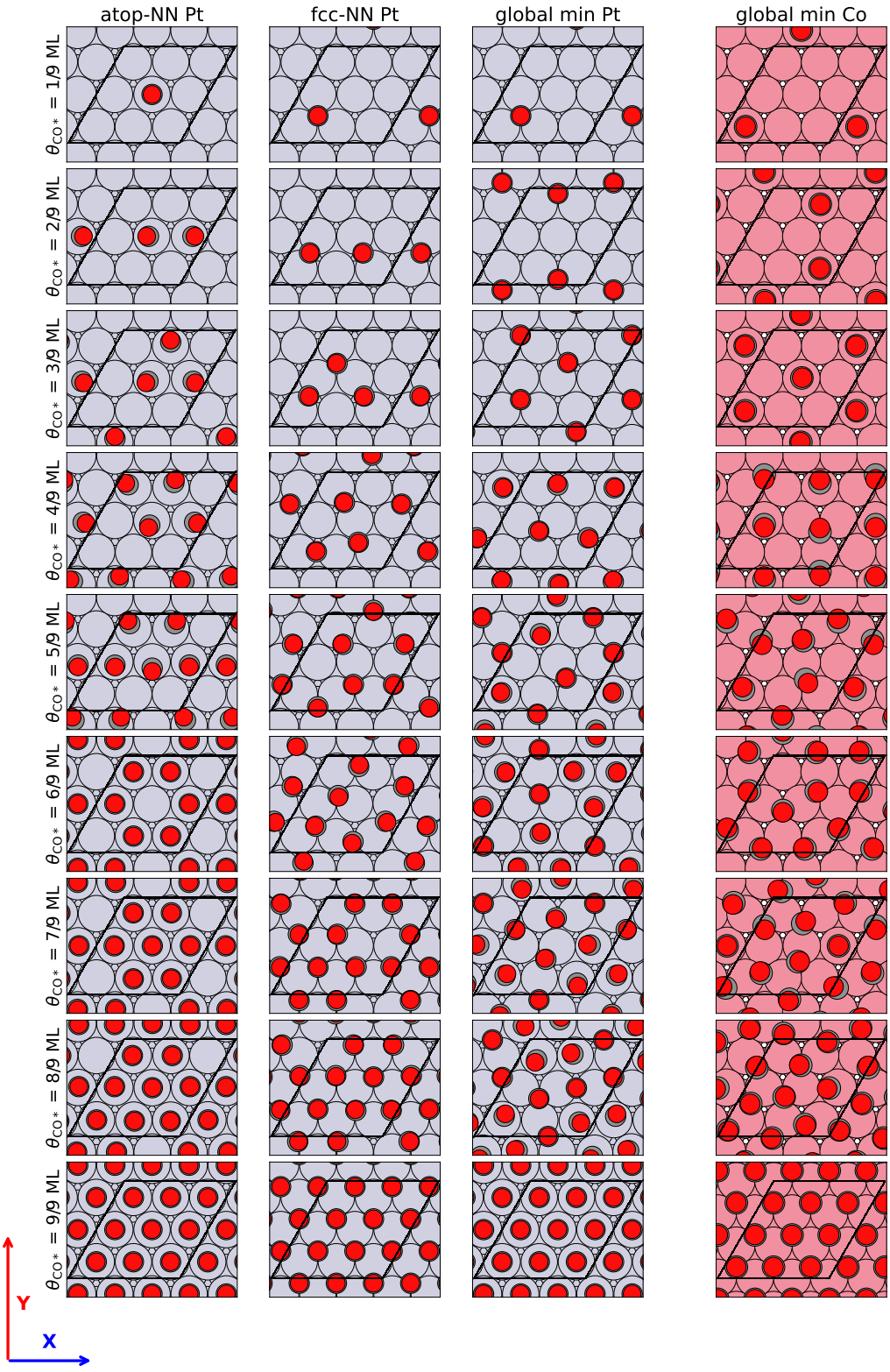

Figure 1: CO*configurations on Pt(111) and Co(0001). Black lines indicate unit cell with periodic boundary condition in xy-plane. Elements in the models are Pt (largest, light gray), Co(pink, large) carbon (medium-sized, dark gray), and oxygen (smallest, red).

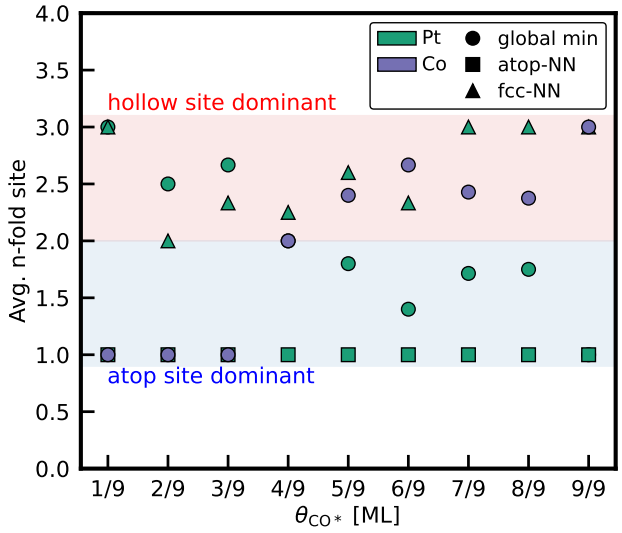

Figure 2: Average n-fold of sites in three configuration models. Values of n-fold each site are atop: 1, bridge: 2, and fcc/hcp hollow: 3.

The adsorption configuration of CO on Co(0001) obtained from the global minima hopping procedure shows the opposite trend compared to the adsorption on Pt(111). In the low coverage limit, CO first occupies atop sites until a coverage of 3/9$^{\text{th}}$ ML is reached. Then, the strong repulsive interaction of CO leads to a destabilization, resulting in the occupation of mostly bridge and 3-fold hollow sites, as seen by the increase in the n-fold value. CO occupies the hcp sites at a full monolayer coverage. From DFT calculations using the revPBE functional, Gunasooriya et al. [87] also observed that CO favors the atop sites until 1/3 ML coverage. Then, adsorption in higher coordinated sites is preferred. However, their most stable configuration at the monolayer coverage is in the bridge site. In our study, we performed relaxations with all CO adsorbates in bridge sites, but the structure always relaxed to the hcp configuration.

The change in the enthalpy of adsorption with coverage for the three configuration models is shown in Figure 1. The CO energy of adsorption was calculated via Equation 14 as an average quantity per CO molecule where E is potential energy and n is the number of CO adsorbate.

$$\Delta E_{\text{ads}}^{\text{CO}^*} = \frac{E^{\text{Pt+n CO}^*} - E^{\text{Pt}} - n\,E^{\text{CO(g)}}}{n} \tag{14}$$

An increasing trend in the adsorption energy as a function of coverage is shown in Figure 3a for Pt(111), indicative of repulsive coverage effects. Based on the shape of the curves, two different regions can be observed: a lesser repulsion at lower coverages, and a greater repulsion at higher coverages. The coverage effect for the low-coverage region is dominated by the adsorbate–surface interaction and the surface relaxation effect, whereas the coverage effect in the high-coverage region is predominantly determined by adsorbate–adsorbate interactions. More specifically, there is an onset of the lateral repulsion among CO* across $\sim$ 0.5 ML, as indicated in Figure S2. Therefore, the addition of lateral repulsion energy on top of the adsorbate–surface interaction and surface relaxation effect is responsible for the increased coverage dependence for $\theta > 0.5$ ML.

Secondly, the calculated adsorption energies for Pt(111) confirm that the global minimum

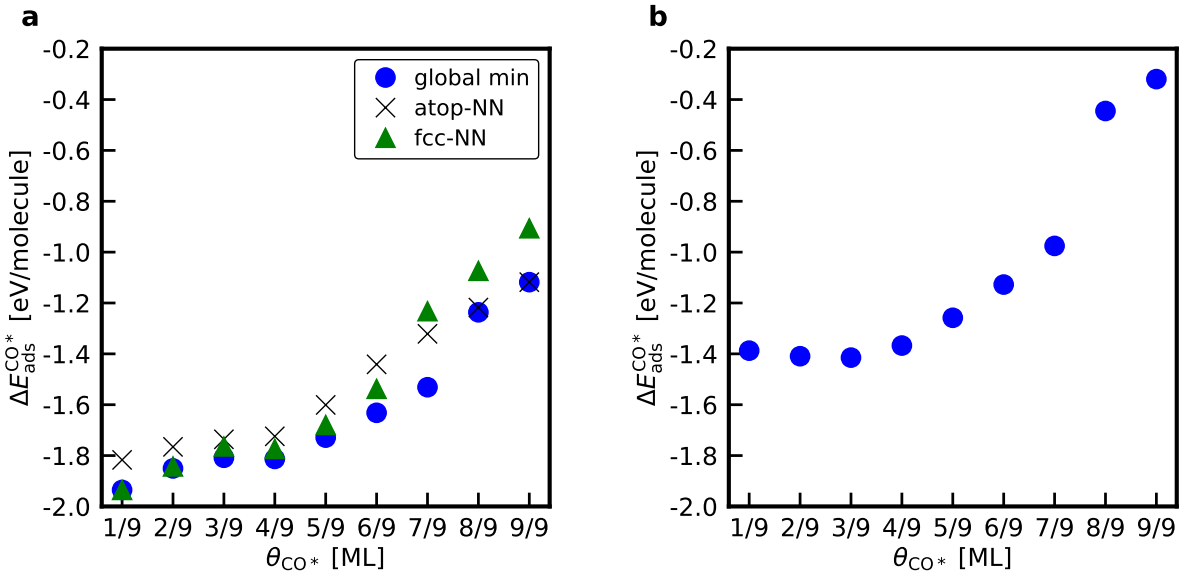

Figure 3: Change in the *CO energy of adsorption as a function of coverage on a) the three configuration models on Pt(111) and b) Co(0001).

model found a lowest energy configuration, noted by the lowest adsorption energy at every coverage. An interesting aspect is that the adsorption energies of the global minimum model appear roughly to be a hybrid of those of the two simplistic models. In the low-coverage region ($\theta <$ 0.5 ML), adsorption energies of global minimum and fcc-NN models are close to each other. In contrast, those of the global minimum and atop-NN energies are similar in the high-coverage region ($\theta >$ 0.5 ML). As coverage increases, we can visually inspect that there is a transition from high-coordination to low-coordination sites in the global minimum model. From this observation, one can speculate this phenomenon is strongly correlated with site-specificity. We can further confirm the site effect based on the global minimum model's site occupancy by categorization with each site's n-fold value. Our model additionally confirmed the occupation of mixed sites as preferred arrangements on Pt, and it confirms that these arrangements will result in lower energy than the occupation of single sites.

The adsorption energy of CO on Co(0001) in Figure 3b also shows a strong repulsive interaction at coverages larger than 4/9 ML. In contrast to Pt(111), CO exhibits attractive interactions at low coverages and reaches a minimum in the binding energy at 1/3 ML, where CO binds more strongly by $3\,\mathrm{kJ\,mol^{-1}}$. At 1/3 ML, CO forms a stable $(\sqrt{3} \times \sqrt{3})R30°$ structure, which has been observed in other theoretical studies and experiments on single crystals [87–89]. From a Natural Bond Order analysis, Gunasooriya et al. [87] concluded that a reduction of electron density in the anti-bonding Co-C orbitals at 1/3 ML leads to the increase in binding energy. The calculated adsorption enthalpy at 1/3 ML is $130\,\mathrm{kJ\,mol^{-1}}$, in good agreement with the experimental value of $128\,\mathrm{kJ\,mol^{-1}}$ [88].

3.2 Coverage dependence on vibrational modes

Our result allows an analysis of experimentally difficult-to-measure low-frequency modes. The six vibrational modes of CO* are visualized in Figure 4. The arrows in Figure 4 aid in the visualization of the modes that move a direction tangential to the surface plane and modes that move in a direction

normal to the surface plane. These six modes were grouped into the four motions by combining similar modes into one to facilitate an analysis. For horizontal motions (or motion in the plane parallel to the surface), the "tilting" motion is where the C atom is relatively stationary and the O atom is moving, while the "pendulum" motion is where the O atom is relatively stationary and the C atom is moving. These four modes are due to the simultaneous frustrated translation (diffusion) of the center of mass and frustrated rotation (libration) about the principal axes. The two vertical motions consist of a desorption mode and an internal stretching mode, which are characterized by changing bond length between Pt−CO and C−O, respectively.

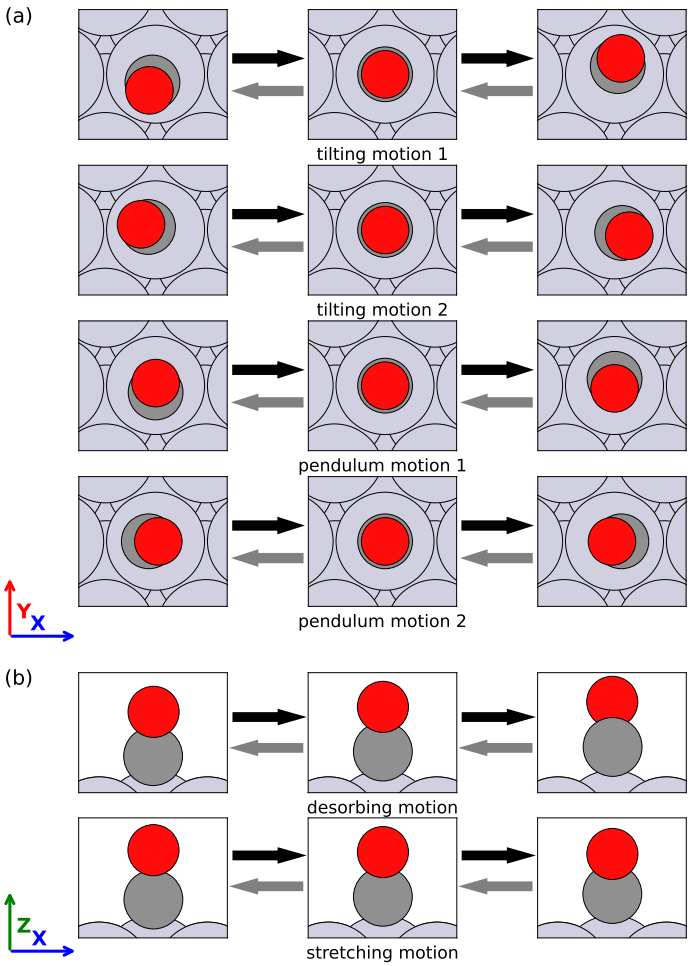

Figure 4: Vibrational modes of CO* on Pt(111) categorized as (a) horizontal motions moving parallel to and (b) vertical motions moving perpendicular to the surface. Each row describes each mode. Elements in the models are Pt (largest, light gray), carbon (medium-sized, dark gray), and oxygen (smallest, red).

The coverage dependence of the vibrational frequencies for both systems is shown in Figure 5 as average values over the number of CO*. By initially focusing our analysis on the atop-NN model's result of Pt(111) in Figure 5a, the site-specific effect can be subtracted since all CO* are exclusively on atop sites. The changes in frequency from 1/9 ML to full coverage were $+152\text{cm}^{-1}$, $+47\text{cm}^{-1}$, -26cm^{-1}, and -45cm^{-1} for tilting, pendulum, desorbing, and stretching motions, re-

spectively. The first observable trend is that the tilting motion is affected most significantly. Similar to the trend in the adsorption energy, both of the horizontal motion frequencies start to increase at 5/9 ML, which was precisely the same coverage at which adsorbate–adsorbate interaction (lateral repulsion) become increasingly repulsive. This result suggests that the horizontal motion frequencies are largely affected by the CO^*-CO^* lateral repulsion, whereas the vertical motions are less significantly influenced by the lateral repulsion. As a consequence of the increased lateral repulsion, the constricted movements in the horizontal direction increased their frequencies.

Secondly, the two vertical motion frequencies decrease with an increasing coverage, while horizontal motion frequencies increases. According to the predictions with vibrational scaling relations developed by Lansford *et al.* [90], the vertical motion vibrational frequency of adsorbed CH_X (X=0-3) on atop sites negatively scales with the adsorption energy (${\omega_{\text{vertical}}}^2 \propto -\Delta E_{\text{ads}}$). Contrarily, the horizontal motion vibrational frequency was reported to be relatively constant with adsorption energy. Our result is in agreement with the literature: as the adsorption energy increases (*i.e.* weaker binding) with the increasing coverage, the frequency of vertical motion decreases. However, the frequency of horizontal motion remains unchanged—regardless of the increased adsorption energy—until the lateral repulsion becomes significant.

Physically, these results make intuitive sense. As the surface becomes increasingly covered, the frustrated translation parallel to the surface becomes increasingly constrained, leading to smaller-amplitude motion and, thus, larger vibrational frequencies with less entropic contribution. Conversely, the weakened binding energy at higher coverages leads to a larger amplitude motion normal to the surface (desorption), thereby lowering the frequency. The trends from the fcc-NN model were consistent with those of atop-NN: relatively mildly affected vertical motions vibrational frequencies and a more noticeable coverage effect in horizontal motions in the higher coverage region.

The global minimum model has an additional effect from the mixed-site occupancy. Like the adsorption energy, vibrational frequencies have a site-dependency, as illustrated in Figure 5e. CO^* adsorbed on atop site has a lower tilting motion frequency, but it has higher pendulum, desorbing, and stretching motion frequencies. Therefore, as the dominant occupancy changes from mainly hollow sites to mainly atop sites, it entails a monotonic increase in pendulum, desorbing, and stretching frequencies. However, the tilting motion frequency showed a decreasing trend in the low-coverage region and an increasing trend in the high-coverage region. This trend is a result of the compound effect of the initial frequency downshift due to the site conversion (hollow site bound $CO^* \rightarrow$ atop site bound CO^*) followed by the frequency upshift due to the lateral repulsion at higher coverages.

Previous investigations hypothesized different explanations for the coverage effect on vibration frequency shifts. The $C-O$ stretching mode was most widely studied since its frequency was in the measurable range by IR spectra. The linearly increasing trend in stretching motion vibrational frequency has long been thought to be due to either intermolecular interaction [13,15] or adsorbate–metal interaction [9, 12]. Instead, our result suggests that the increasing stretching frequency trend stems from the site conversion from a more hollow site to a more atop site with increasing coverage. On the other hand, for the horizontal motion, we propose that both site conversion and lateral repulsion induce the frequency change.

The vibrational modes of the tilting motion initially decrease for CO adsorbed on Co(0001) in the $(\sqrt{3} \times \sqrt{3})R30^\circ$ structure at 1/3 ML coverage. At higher coverages, the vibrational modes follow the trend from Pt(111); the modes increase as the motion becomes restricted by the co-adsorbates. Pendulum and desorbing modes remain relatively constant until a coverage of 5/9 ML,

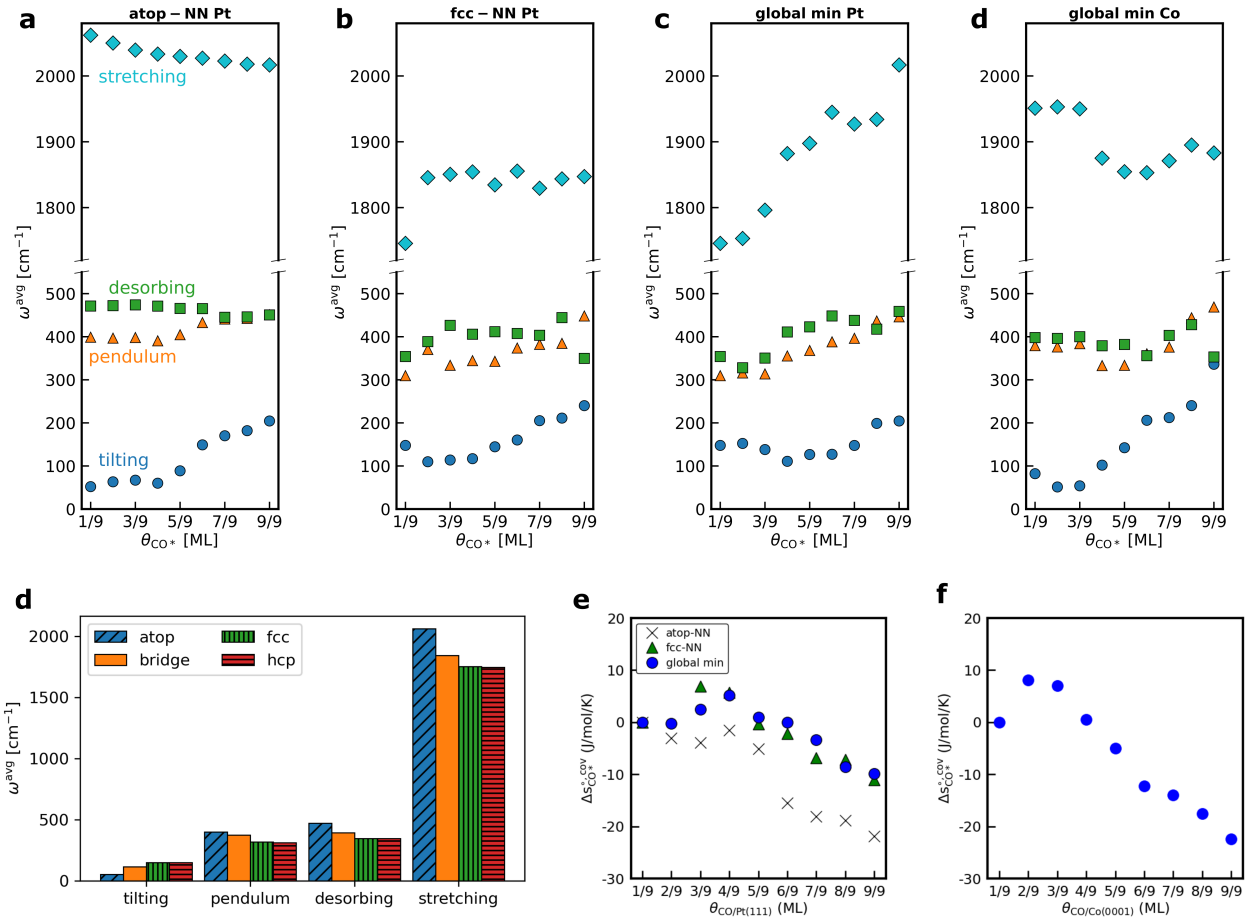

Figure 5: Average vibrational frequencies of four vibrational motions of CO* as a function of coverage for Pt(111) with the configurations from a) atop-NN, b) fcc-NN, and c) global minima hopping. d) Average vibrational frequencies for CO on Co(0001). e) Average vibrational frequencies of CO* at four binding sites of Pt(111) at $\theta = 1/9$ ML. CO* coverage-dependent entropy evaluated at the standard state of 298.15 K and 1 bar on f) Pt(111) and g) Co(0001). Entropies are with respect to the value in the low-coverage limit.

but then also increase with coverage. The change in the C-O stretching frequency can be correlated with the adsorption site. Up to 1/3 ML, CO is exclusively adsorbed on atop sites and the stretching frequency remains constant. At 4/9 ML CO, moves to sites with higher-coordination numbers and the stretching mode decreases by 100 wave numbers. The occupation of bridge and 3-fold hollow sites leads to a decrease of the stretching mode, which is also confirmed by the results on Pt(111).

The vibrational frequencies obtained from DFT were used in partition functions for harmonic oscillators, from which the vibrational entropy was obtained, both for the low-coverage limit and for the coverage-dependent correction. Coverage influences the entropy of adsorbed CO on Pt(111) and Co(0001) derived from the structures of the global minimum method similarly (see Figure 5f,g). First, the entropy increases, which is a consequence of the decreasing low-frequency tilting modes up to a coverage of 4/9 ML for Pt(111) and 1/3 ML for Co(0001). The entropy decreases by $10\,\mathrm{J\,mol^{-1}\,K^{-1}}$ on Pt(111) at 1 ML CO coverage, whereas on Co(0001) the entropy decreases by $25\,\mathrm{J\,mol^{-1}\,K^{-1}}$.

Although the present work is focused on the impact of coverage on normal modes, the vibrational partition function is not the only source of entropy for an adsorbate. The various possible configurations of adsorbates on a lattice also contribute to the overall entropy. In the case of ideal (non-interacting) adsorbates, the partial molar configurational entropy is given by the well-known formula $\overline{s}_{\mathrm{config}} = -k_{\mathrm{B}}\ln\frac{\theta}{1-\theta}$ (see SI for a derivation) [4,7,72,91–95]. An underlying assumption in this derivation is that all the combinatorial ways of arranging adsorbates result in the same energy. When lateral interactions are considered, however, this assumption is no longer applicable; the energy will vary—often considerably—with different arrangements. When the energies are not equal, the configurational partition function should be composed of both degeneracies and Boltzmann factors [7]. The demanding task of linking the configurational degeneracy and the energetics makes accurate quantification of the configurational contribution challenging [96]. Furthermore, the inhomogeneity of sites present even on simple metallic surfaces will bring in an additional layer of complexity. A more proper quantification of configurational entropy under non-ideal conditions will be the subject of forthcoming work. However, in the present study, we neglect the configurational contribution, but we acknowledge that it is certainly a crucial aspect to improve upon in the future.

3.3 Effect of coverage-dependent thermochemistry on equilibrium and transient prediction

Inclusion of coverage-dependent thermodynamic parameters via analytical expressions, as opposed to evaluating thermochemistry on the fly during the kinetic modeling, has two benefits. First, it is computationally more efficient. Second, this approach helps to alleviate the patchiness of the discrete data due to the finite unit cell size and achieves more smooth and continuous profiles in MKM. We focus only on the results obtained from the global minima hopping for Pt(111) and Co(0001) for the microkinetic modeling. The coverage dependence was parameterized with continuous forms with the four algebraic models, as illustrated in Figure 6a, and the parameters for each model are listed in the SI. For the coverage-dependent heat capacity, which has an additional temperature dependence, a log-quadratic model (Equation 11) was fitted as shown in Figure S6. The parameterized properties for atop-NN and fcc-NN are provided in SI.

Equilibrium simulations were conducted with the coverage-dependent thermodynamic properties. Adsorption isotherms for CO adsorption on Pt(111) at three different temperatures are shown

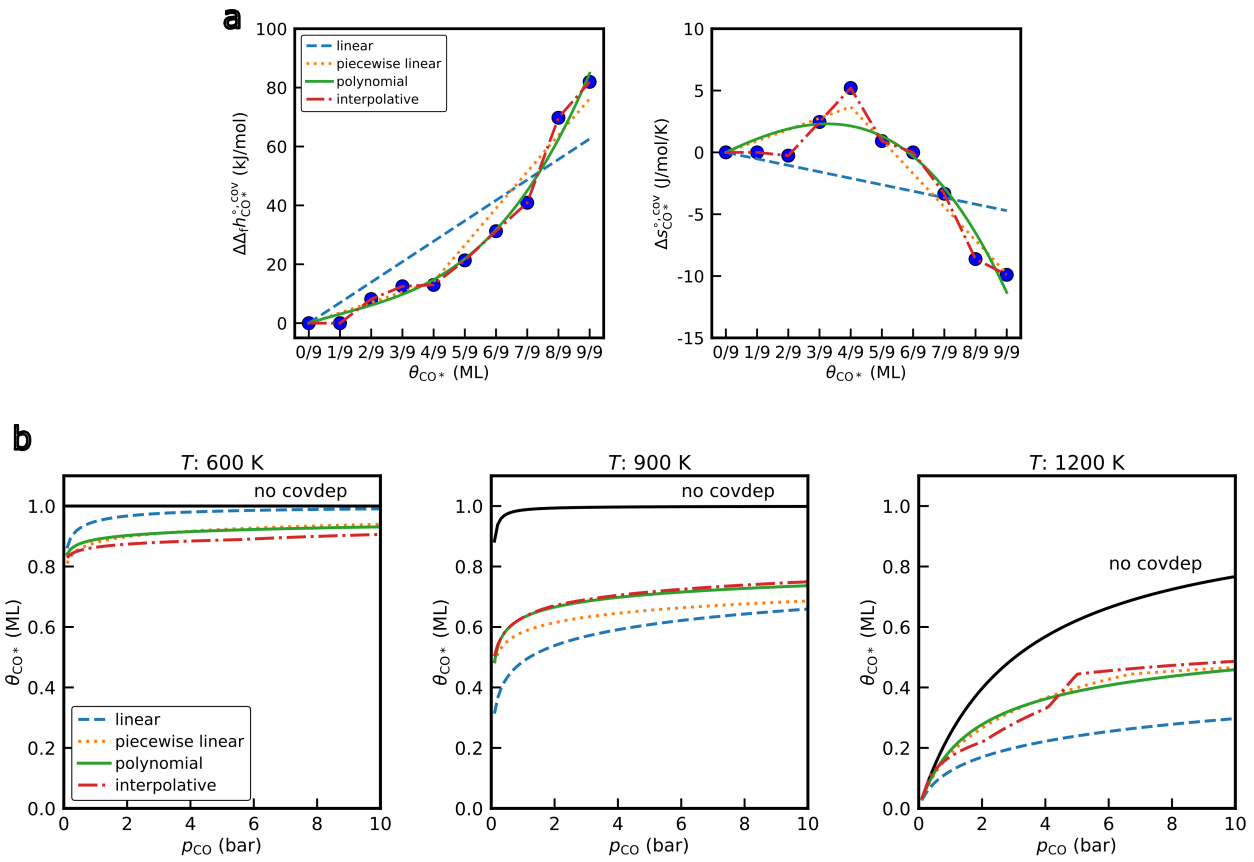

Figure 6: a) Fitted algebraic equations of the CO* coverage-dependent change in enthalpy of formation and change in entropy on Pt(111) calculated with the global minimum configuration results. b) CO adsorption isotherms with four dependency models fitted on global minimum result at 600 K, 900 K, and 1200 K. The red solid curve in b, c shows an idealized case assuming no coverage dependence.

in Figure 6b. Additional transient simulations for the CO oxidation in a batch reactor are provided in the SI. For all the tested temperatures, especially for higher temperatures, the coverage-dependent models resulted in noticeably different isotherms from the ideal-adsorbate model (*i.e.* no coverage effect model). Among them, we considered the interpolative model isotherm as the most accurate standard—at a minimum they are exact at the nine discrete coverages. The linear model isotherm is furthest away from the interpolative model isotherm. This discrepancy is due to the oversimplification of the coverage dependence as shown by a conspicuous over/under predicting in Figure 6. The piecewise linear and polynomial model isotherms simulate the interpolative isotherm much more closely. However, jagged features in piecewise linear and interpolative models (Figure 6a) propagated to their isotherms at 1200 K. The jagged features become apparent at 1200 K because the coverage changes from 0 to 0.5, whereas it remains relatively constant for the lower temperatures. Due to the relatively constant coverage at low temperatures, the coverage-dependence polynomial is in the linear part of the interpolative model resulting to the absence of kinks. Although our piecewise linear isotherm is subtly kinked, the piecewise linear model was reported by Bajpai *et al.* [38] to render discontinuous predictions. Therefore, the polynomial model is recommended based on its good balance between accuracy and smooth, continuous profile.

3.4 Impact of coverage-dependent vibrational entropy

The previous results demonstrated that the lateral interactions have a substantial impact on the thermophysical properties of adsorbates and, thence, the free energies of the system. In this section, we aim to disentangle the enthalpic and entropic contributions to the coverage-dependent free energy. Figure 7 shows van't Hoff diagrams of the equilibrium constant of the CO adsorption on Pt(111) and Co(0001). For the CO/Pt(111) system, the lateral interactions are only repulsive, increasing the free energy of formation and decreasing the equilibrium constant. A coverage-dependent entropy has only modest effects on the equilibrium constant (see Figure 7a,b).

The results are different for CO adsorbed on Co(0001) in Figure 7c. Due to the attractive interactions at a coverage of 1/3 ML, the equilibrium constant first increases with increasing coverage before the repulsive interactions become dominating. The impact of entropy is much more pronounced. An omission of coverage dependence leads to an equilibrium constant that deviates by orders of magnitude at high coverages. The importance of accurately quantifying the attractive interactions at medium coverages becomes apparent when comparing the relative equilibrium constants in Figure 7d. The formation of the stabilized $(\sqrt{3} \times \sqrt{3})R30°$-CO islands increases the adsorption equilibrium constant by a factor of 3–7, depending on the temperature when coverage effects for the enthalpy and entropy are considered. Without the inclusion of a coverage-dependent entropy, K_{eq} increases only by a factor 1.5–2.2. The inclusion of the entropy effects for the accurate modeling of the CO coverage on Co(0001) is crucial since the *CO coverage controls the chain growth in the Fischer-Tropsch process [97].

The adsorption isotherms for on Pt(111) and the transient simulations in Figure 6 included both enthalpic and entropic contributions. In an effort to compare the relative magnitude, we include only one effect at a time, either coverage-dependent enthalpy or coverage-dependent entropy, and evaluated the results independently. Due to the aforementioned desired features of the polynomial dependency model, it was used exclusively for the analysis in this section.

In Figure 8, the decoupled effects in equilibrium prediction are shown. Each coverage effect was quantified as a deviation from the ideal model. For all temperatures, the effect of enthalpic coverage dependence was greater relative to the effect of entropic coverage dependence, up to about 4 times. Aside from the relatively low entropic contribution, it could be seen that the effect can be important at high temperatures, as expected with the $-TS$ term in the free energy evaluation.

Figure 9 shows the result from the transient simulations of the TPD profiles. Instead of showing the differences, two different curves were plotted along with the ideal model, with only enthalpic coverage effects and with both effects. The TPD profiles from Pt(111) and Co(0001) demonstrate that the enthalpic coverage effect is substantially more impactful, shown by not only the deviation from the ideal assumption profile but also by its proximity to the profile with both effects. Including a coverage-dependent enthalpy shifts the onset of desorption and the peak to lower temperatures for the Pt(111) facet. While the onset is also shifted to lower temperatures for Co(0001), the maximum desorption rate is observed at higher temperatures compared to the ideal case. This shift to higher temperatures clearly displays the stabilizing interactions of CO on Co(0001) in the form of the $(\sqrt{3} \times \sqrt{3})R30°$ structure. Additionally, the significance of a coverage-dependent entropy is more pronounced for Co(0001) than for Pt(111).

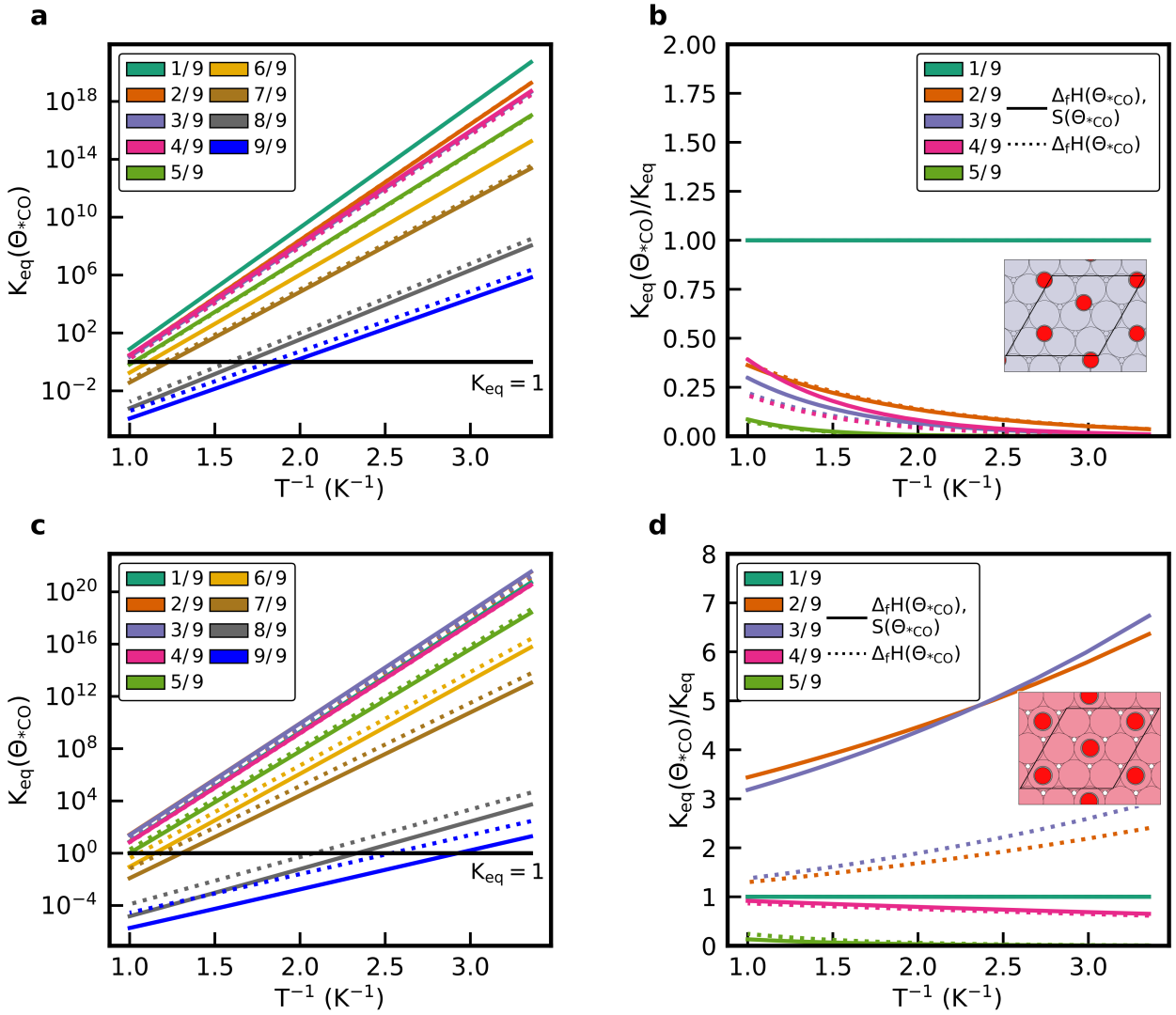

Figure 7: Evaluation of the impact of coverage-dependent entropy on the equilibrium constant for the adsorption of CO. a) Van't Hoff diagram for the adsorption on Pt(111) at various coverages. b) Equilibrium constant normalized to the equilibrium constant in the low coverage limit for Pt(111). c) Van't Hoff diagram for the adsorption on Co(111) at various coverages. b) Equilibrium constant normalized to the equilibrium constant in the low coverage limit for Co(111). The dashed line are the results with only a coverage-dependent enthalpy and the solid line contains the results with coverage-dependent enthalpy and entropy.

3.5 Discussion

The conclusion that enthalpic effects are more important than entropic effects is hardly surprising. Nevertheless, the present work provides some useful context in the consideration of coverage-dependent entropy. The impact of lateral interactions on vibrational entropy is expected to be important for large-amplitude, low-frequency normal modes, such as those that describe the frustrated diffusion and libration parallel to the surface. The impact is expected to be dependent on both the binding energy and the binding site. As the surface coverage increases, repulsive interactions

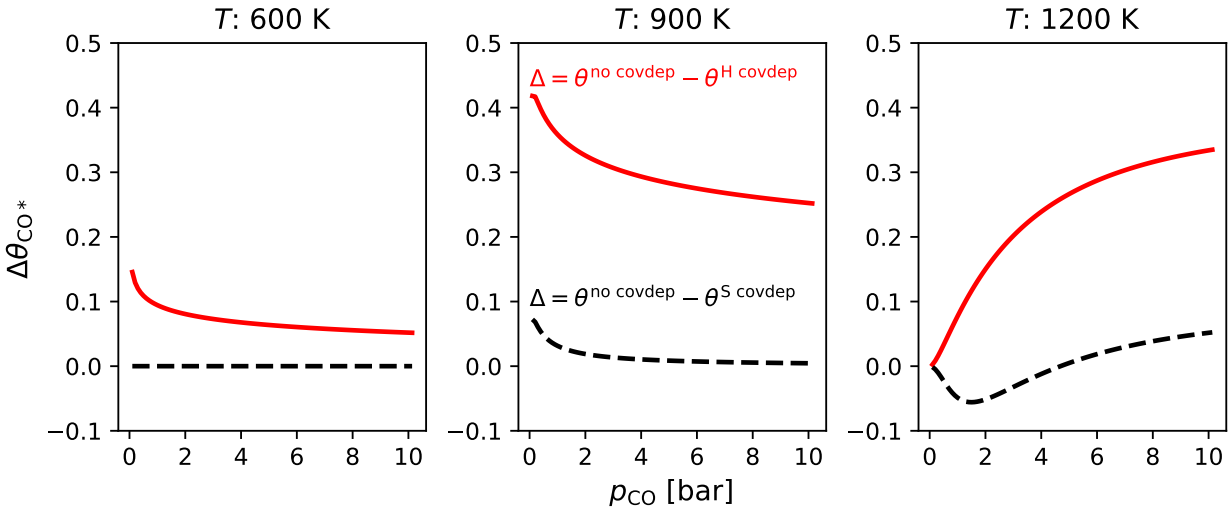

Figure 8: Contributions of enthalpic and entropic coverage effects on the adsorption isotherm of CO on Pt(111) illustrated as the deviation from the ideal at 600 K, 900 K, and 1200 K and 1 bar.

should lead to a crowding effect that should reduce the area available for large-amplitude motion, thereby increasing the vibrational frequency and thus decreasing the entropy. In some instances, however, the opposite effect occurred; the increased crowding caused a shift to other binding sites with lower frequency modes, thereby increasing the vibrational entropy. Hence, the vibrational entropy for loosely bound adsorbates could be highly dependent on coverage. Similarly, for an adsorbate with a strong dipole moment such as SO_2 [98], the coverage effect on lateral motion frequencies is anticipated to be much greater. Additionally, it will also be necessary to include cross interactions in the form of higher-order terms into the coverage-dependence thermochemistry model to achieve a more accurate description of the enthalpy and entropy at high coverages [34,99], which is the subject of future work.

More generally, the present work provides a better conceptual understanding of the interplay between lateral interactions and entropy. Based upon the present work, we conclude that the significance of coverage-dependent entropy is constrained by thermodynamics at both low and high temperatures. At low temperatures, the surface is completely saturated and coverage effects are critical. However, at low-temperature conditions, the free energy is dominated by enthalpy, and entropic considerations are generally negligible. Conversely, at high temperatures, entropic effects can be the dominant term for the free energy, but the coverage is expected to be low because the dominant driving force is desorption. Accordingly, there is a narrow window in which the temperature is high enough that entropic effects are important, but low enough that the surface is still crowded. The limits of this window will be system specific.

Finally, we wish to emphasize that these conclusions were possible only because of the easy parameterization of coverage-dependent thermophysical properties in Cantera. The ability to include coverage-dependent binding energies in a systematic, robust method that does not violate thermodynamic consistency has proven itself indispensable for mean-field models in computational heterogeneous catalysis [40,41,83,84].

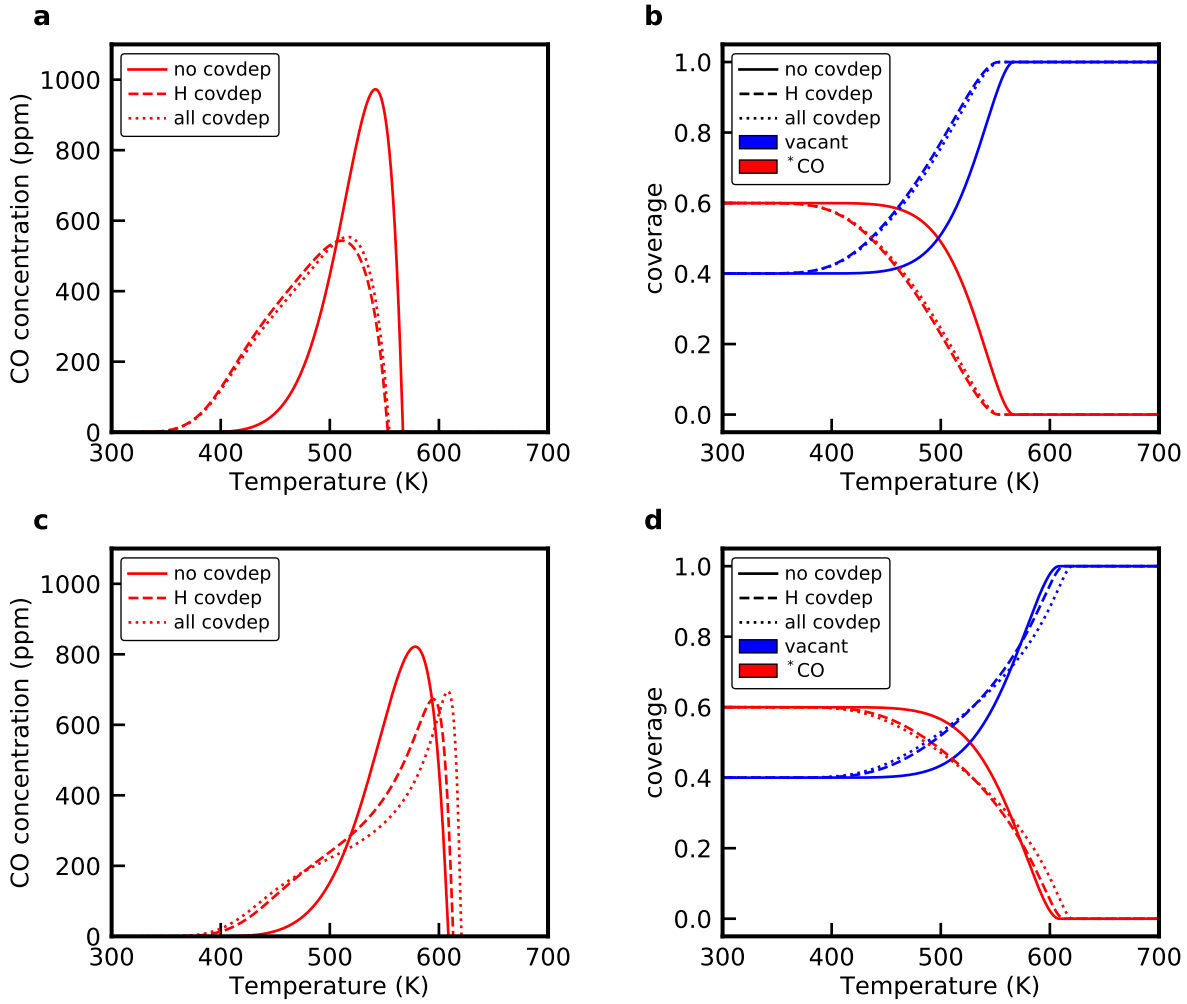

Figure 9: CO temperature-programmed desorption profile from a) Pt(111) with the corresponding coverage profiles in b) and c) Co(0001) with the corresponding coverage profiles in d). *Conditions:* $T = 300\,\mathrm{K}$, $\Theta_{*CO,0} = 0.6$ ML

4 Conclusions

A novel procedure for quantifying the impact of lateral interactions on the thermophysical properties of adsorbates is presented. The procedure includes four different models to parameterize the contribution of coverage dependence on the enthalpy, entropy, and heat capacity of adsorbates. It was observed that, of the four different models, the polynomial model was superior to the others in that it results in a smooth function that nonetheless captures the non-linear response of enthalpy and entropy to surface crowding. These new coverage-dependent functions were tested on two systems: CO/Pt(111) and CO/Co(0001). A two-slope trend was observed for coverage-dependent adsorption energy. Our analysis implies this two-step coverage effect is a result of a transition from solely indirect adsorbate–metal interaction and surface relaxation effect for the lower coverages to combined indirect and direct adsorbate–adsorbate interactions for the higher coverages. The change in vibrational entropy as a function of coverage was rationalized in terms of changes to low-frequency modes. Depending upon the specific adsorbate, its binding energy, and its preferred binding site,

the vibrational entropy can either increase or decrease with increasing coverage at lower coverages, but at higher coverages, the increase in repulsive interactions leads to a net reduction in entropy. The impact of coverage on enthalpy was more significant than the impact of coverage on entropy. Using basic thermodynamic arguments, we conclude that coverage-dependent entropic effects are confined to a narrow temperature regime. These coverage-dependent models are now available in Cantera. The resulting microkinetic mechanisms are thermodynamically consistent.

ASSOCIATED CONTENT

Supporting information. In the supporting information, (1) configurational entropy with no lateral interaction, (2) diffusion barrier of CO*, (3) adsorbate–adsorbate interaction potential, (4) site-specific energy of adsorption, (5) parameterized coverage dependence for atop-NN and fcc-NN, (6) adorption isotherm and batch simulation with atop-NN and fcc-NN coverage dependence, (7) coverage-dependent entropic contribution in atop-NN and fcc-NN predictions, (8) prediction comparison simplistic models are included. (9) Microkinetic mechanism with each coverage dependence, in Cantera format, is also included.

AUTHOR INFORMATION

Corresponding authors. *Email: andrew_peterson@brown.edu. Telephone +1 401-863-2153. *Email: franklin_goldsmith@brown.edu. Telephone +1 401-863-6468.

Acknowledgments. This work was sponsored by the National Science Foundation, Office of Advanced Cyberinfrastructure, through award number OAC-1931397. AAP and CFG gratefully acknowledge additional financial support from the U.S. Department of Energy, Office of Science, Basic Energy Sciences, Chemical Sciences, Geosciences and Biosciences Division, as part of the Computational Chemistry Sciences Program, through award number DE-SC0019441, with Dr. Aaron Holder as the program manager. We also thank Dr. Raymond Speth and Dr. Bryan Weber for their invaluable help on implementation of coverage-dependent thermochemistry in Cantera.

References

[1] Wehinger, G.D.; Ambrosetti, M.; Cheula, R.; Ding, Z.B.; Isoz, M.; Kreitz, B.; Kuhlmann, K.; Kutscherauer, M.; Niyogi, K.; Poissonnier, J.; Réocreux, R.; Rudolf, D.; Wagner, J.; Zimmermann, R.; Bracconi, M.; Freund, H.; Krewer, U.; Maestri, M. Quo Vadis Multiscale Modeling in Reaction Engineering? – A Perspective. *Chemical Engineering Research and Design* **2022**; 184, 39–58.

[2] Bruix, A.; Margraf, J.T.; Andersen, M.; Reuter, K. First-Principles-Based Multiscale Modelling of Heterogeneous Catalysis. *Nature Catalysis* **2019**; 2, 659–670.

[3] Langmuir, I. The constitution and fundamental properties of solids and liquids. Part I. Solids. *Journal of the American Chemical Society* **1916**; 38, 2221–2295.

[4] Fowler, R.; Guggenheim, E.A. *Statistical Thermodynamics*. Cambridge University Press, Cambridge **1939**.

[5] Temkin, M.; Pyzhev, V. Kinetics of Ammonia Synthesis on Promoted Iron Catalyst. *Acta physicochimica U.R.S.S.* **1940**; 12, 327–355.

[6] Hinshelwood, C. *The kinetics of chemical change*. The Clarendon press, Oxford **1940**.

[7] Everett, D.H. The thermodynamics of adsorption: Part II. - Thermodynamics of monolayers on solids. *Transactions of the Faraday Society* **1950**; 46, 942–957.

[8] Boudart, M.; Djéga-Mariadassou, G. *Kinetics of Heterogeneous Catalytic Reactions*. Princeton University Press **1984**.

[9] Blyholder, G. Molecular Orbital View of Chemisorbed Carbon Monoxide. *The Journal of Physical Chemistry* **1964**; 68, 2772–2777.

[10] Grimley, T.; Walker, S. Interactions between adatoms on metals and their effects on the heat of adsorption at low surface coverage. *Surface Science* **1969**; 14, 395–406.

[11] Einstein, T.L.; Schrieffer, J.R. Indirect Interaction between Adatoms on a Tight-Binding Solid. *Physical Review B* **1973**; 7, 3629–3648.

[12] Bradshaw, A.; Hoffmann, F. The chemisorption of carbon monoxide on palladium single crystal surfaces: IR spectroscopic evidence for localised site adsorption. *Surface Science* **1978**; 72, 513–535.

[13] Scheffler, M. The influence of lateral interactions on the vibrational spectrum of adsorbed CO. *Surface Science* **1979**; 81, 562–570.

[14] Ortega, A.; Huffman, F.M.; Bradshaw, A.M. The adsorption of CO on Pd(100) studied by IR reflection absorption spectroscopy. *Surface Science* **1982**; 119, 79–94.

[15] Ueba, H. Chemical effects on vibrational properties of adsorbed molecules on metal surfaces: Coverage dependence. *Surface Science* **1987**; 188, 421–455.

[16] Persson, B.N. Monte Carlo calculations of adsorbate structures and the role of the vibrational entropy in phase transitions at surfaces. *Physical Review B* **1989**; 40, 7115–7123.

[17] Hammer, B.; Morikawa, Y.; Nørskov, J.K. CO Chemisorption at Metal Surfaces and Overlayers. *Physical Review Letters* **1996**; 76, 2141–2144.

[18] Hammer, B. Coverage dependence of N2 dissociation at an N, O, or H precovered Ru(0001) surface investigated with density functional theory. *Physical Review B - Condensed Matter and Materials Physics* **2001**; 63, 1–8.

[19] Dohnálek, Z.; Kim, J.; Bondarchuk, O.; Mike White, J.; Kay, B.D. Physisorption of N2, O2, and CO on fully oxidized TiO2(110). *Journal of Physical Chemistry B* **2006**; 110, 6229–6235.

[20] Mason, S.E.; Grinberg, I.; Rappe, A.M. Adsorbate-adsorbate interactions and chemisorption at different coverages studied by accurate ab initio calculations: CO on transition metal surfaces. *Journal of Physical Chemistry B* **2006**; 110, 3816–3822.

[21] Mortensen, J.; Hammer, B.; Nørskovi, J. A Theoretical Study of Adsorbate–Adsorbate Interactions on Ru(0001). *Surface Science* **1998**; 414, 315–329.

[22] Eischens, R.P.; Francis, S.A.; Pliskin, W.A. The Effect of Surface Coverage on the Spectra of Chemisorbed CO. *The Journal of Physical Chemistry* **1956**; 60, 194–201.

[23] Shigeishi, R.; King, D.A. Chemisorption of carbon monoxide on platinum {111}: Reflection-absorption infrared spectroscopy. *Surface Science* **1976**; 58, 379–396.

[24] Surnev, L.; Xu, Z.; Yates, J.T. IRAS study of the adsorption of CO on Ni(111): Interrelation between various bonding modes of chemisorbed CO. *Surface Science* **1988**; 201, 1–13.

[25] Campbell, C.T. Atomic and molecular oxygen adsorption on Ag(111). *Surface Science* **1985**; 157, 43–60.

[26] Diekhöner, L.; Mortensen, H.; Baurichter, A.; Luntz, A.C. Coverage dependence of activation barriers: Nitrogen on Ru(0001). *Journal of Vacuum Science & Technology A: Vacuum, Surfaces, and Films* **2000**; 18, 1509–1513.

[27] Getman, R.B.; Schneider, W.F.; Smeltz, A.D.; Delgass, W.N.; Ribeiro, F.H. Oxygen-coverage effects on molecular dissociations at a Pt metal surface. *Physical Review Letters* **2009**; 102, 9–12.

[28] Smirnov, K.S.; Raseev, G. Coverage dependent IR frequency shift of CO molecules adsorbed on Ni(111) surface. *Surface Science* **1997**; 384.

[29] Aizawa, H.; Morikawa, Y.; Tsuneyuki, S.; Fukutani, K.; Ohno, T. A density-functional study of the atomic structures and vibrational spectra of NO/Pt(1 1 1). *Surface Science* **2002**; 514, 394–403.

[30] Deshlahra, P.; Conway, J.; Wolf, E.E.; Schneider, W.F. Influence of Dipole–Dipole Interactions on Coverage-Dependent Adsorption: CO and NO on Pt(111). *Langmuir* **2012**; 28, 8408–8417.

[31] McEwen, J.S.; Payne, S.H.; Kreuzer, H.J.; Kinne, M.; Denecke, R.; Steinrück, H.P. Adsorption and desorption of CO on Pt(1 1 1): A comprehensive analysis. *Surface Science* **2003**; 545, 47–69.

[32] Tang, H.; Van Der Ven, A.; Trout, B.L. Phase diagram of oxygen adsorbed on platinum (111) by first-principles investigation. *Physical Review B - Condensed Matter and Materials Physics* **2004**; 70, 1–10.

[33] Mhadeshwar, A.B.; Kitchin, J.R.; Barteau, M.A.; Vlachos, D.G. The role of adsorbate-adsorbate interactions in the rate controlling step and the most abundant reaction intermediate of NH_3 decomposition on RU. *Catalysis Letters* **2004**; 96, 13–22.

[34] Grabow, L.C.; Hvolbæk, B.; Nørskov, J.K. Understanding Trends in Catalytic Activity: The Effect of Adsorbate–Adsorbate Interactions for CO Oxidation Over Transition Metals. *Topics in Catalysis* **2010**; 53, 298–310.

[35] Stamatakis, M.; Chen, Y.; Vlachos, D.G. First-principles-based kinetic Monte Carlo simulation of the structure sensitivity of the water-gas shift reaction on platinum surfaces. *Journal of Physical Chemistry C* **2011**; 115, 24750–24762.

[36] Wu, C.; Schmidt, D.J.; Wolverton, C.; Schneider, W.F. Accurate coverage-dependence incorporated into first-principles kinetic models: Catalytic NO oxidation on Pt (1 1 1). *Journal of Catalysis* **2012**; 286, 88–94.

[37] Lausche, A.C.; Medford, A.J.; Khan, T.S.; Xu, Y.; Bligaard, T.; Abild-Pedersen, F.; Nørskov, J.K.; Studt, F. On the effect of coverage-dependent adsorbate–adsorbate interactions for CO methanation on transition metal surfaces. *Journal of Catalysis* **2013**; 307, 275–282.

[38] Bajpai, A.; Frey, K.; Schneider, W.F. Comparison of Coverage-Dependent Binding Energy Models for Mean-Field Microkinetic Rate Predictions. *Langmuir* **2020**; 36, 465–474.

[39] Li, X.; Grabow, L.C. Evaluating the benefits of kinetic Monte Carlo and microkinetic modeling for catalyst design studies in the presence of lateral interactions. *Catalysis Today* **2022**; 387, 150–158.

[40] Kreitz, B.; Wehinger, G.D.; Goldsmith, C.F.; Turek, T. Microkinetic Modeling of the Transient CO_2 Methanation with DFT-Based Uncertainties in a Berty Reactor. *ChemCatChem* **2022**; 202200570.

[41] Kreitz, B.; Lott, P.; Bae, J.; Blöndal, K.; Angeli, S.; Ulissi, Z.W.; Studt, F.; Goldsmith, C.F.; Deutschmann, O. Detailed Microkinetics for the Oxidation of Exhaust Gas Emissions through Automated Mechanism Generation. *ACS Catalysis* **2022**; , 11137–11151.

[42] Goswami, A.; Ma, H.; Schneider, W.F. Consequences of Adsorbate-Adsorbate Interactions for Apparent Kinetics of Surface Catalytic Reactions. *Journal of Catalysis* **2022**; 405, 410–418.

[43] Nolen, M.A.; Farberow, C.A.; Kwon, S. Incorporating Coverage-Dependent Reaction Barriers into First-Principles-Based Microkinetic Models: Approaches and Challenges. *ACS Catalysis* **2024**; , 14206–14218.

[44] Matera, S.; Schneider, W.F.; Heyden, A.; Savara, A. Progress in Accurate Chemical Kinetic Modeling, Simulations, and Parameter Estimation for Heterogeneous Catalysis. *ACS Catalysis* **2019**; 9, 6624–6647.

[45] Zijlstra, B.; Broos, R.J.P.; Chen, W.; Bezemer, G.L.; Filot, I.A.W.; Hensen, E.J.M. The Vital Role of Step-Edge Sites for Both CO Activation and Chain Growth on Cobalt Fischer–Tropsch Catalysts Revealed through First-Principles-Based Microkinetic Modeling Including Lateral Interactions. *ACS Catalysis* **2020**; 10, 9376–9400.

[46] Klumpers, B.; Hensen, E.J.; Filot, I.A. Lateral Interactions of Dynamic Adlayer Structures from Artificial Neural Networks. *The Journal of Physical Chemistry C* **2022**; 126, 5529–5540.

[47] Dietze, E.M.; Grönbeck, H. Ensemble Effects in Adsorbate–Adsorbate Interactions in Microkinetic Modeling. *Journal of Chemical Theory and Computation* **2023**; 19, 1044–1049.

[48] Goswami, A.; Schneider, W.F. Mean Field Model Parameterization to Recover Coverage-Dependent Kinetics. *Journal of Catalysis* **2023**; 426, 352–360.

[49] Maestri, M.; Vlachos, D.; Beretta, A.; Groppi, G.; Tronconi, E. Steam and Dry Reforming of Methane on Rh: Microkinetic Analysis and Hierarchy of Kinetic Models. *Journal of Catalysis* **2008**; 259, 211–222.

[50] Chan, D.; Tischer, S.; Heck, J.; Diehm, C.; Deutschmann, O. Correlation between Catalytic Activity and Catalytic Surface Area of a Pt/Al2O3 DOC: An Experimental and Microkinetic Modeling Study. *Applied Catalysis B: Environmental* **2014**; 156–157, 153–165.

[51] Delgado, K.; Maier, L.; Tischer, S.; Zellner, A.; Stotz, H.; Deutschmann, O. Surface Reaction Kinetics of Steam- and CO2-Reforming as Well as Oxidation of Methane over Nickel-Based Catalysts. *Catalysts* **2015**; 5, 871–904.

[52] Salciccioli, M.; Chen, Y.; Vlachos, D.G. Microkinetic Modeling and Reduced Rate Expressions of Ethylene Hydrogenation and Ethane Hydrogenolysis on Platinum. *Industrial & Engineering Chemistry Research* **2011**; 50, 28–40.

[53] Mhadeshwar, A.B.; Wang, H.; Vlachos, D.G. Thermodynamic Consistency in Microkinetic Development of Surface Reaction Mechanisms. *The Journal of Physical Chemistry B* **2003**; 107, 12721–12733.

[54] Wehinger, G.D.; Kraume, M.; Berg, V.; Korup, O.; Mette, K.; Schlögl, R.; Behrens, M.; Horn, R. Investigating dry reforming of methane with spatial reactor profiles and particle-resolved CFD simulations. *AIChE Journal* **2016**; 62, 4436–4452.

[55] Medford, A.J.; Shi, C.; Hoffmann, M.J.; Lausche, A.C.; Fitzgibbon, S.R.; Bligaard, T.; Nørskov, J.K. CatMAP: A Software Package for Descriptor-Based Microkinetic Mapping of Catalytic Trends. *Catalysis Letters* **2015**; 145, 794–807.

[56] Goodwin, D.G.; Speth, R.L.; Moffat, H.K.; Weber, B.W. Cantera: An Object-oriented Software Toolkit for Chemical Kinetics, Thermodynamics, and Transport Processes. `https://www.cantera.org` **2021**.

[57] Giannozzi, P.; Baroni, S.; Bonini, N.; Calandra, M.; Car, R.; Cavazzoni, C.; Ceresoli, D.; Chiarotti, G.L.; Cococcioni, M.; Dabo, I.; Dal Corso, A.; De Gironcoli, S.; Fabris, S.; Fratesi, G.; Gebauer, R.; Gerstmann, U.; Gougoussis, C.; Kokalj, A.; Lazzeri, M.; Martin-Samos, L.; Marzari, N.; Mauri, F.; Mazzarello, R.; Paolini, S.; Pasquarello, A.; Paulatto, L.; Sbraccia, C.; Scandolo, S.; Sclauzero, G.; Seitsonen, A.P.; Smogunov, A.; Umari, P.; Wentzcovitch, R.M. QUANTUM ESPRESSO: A modular and open-source software project for quantum simulations of materials. *Journal of Physics Condensed Matter* **2009**; 21.

[58] Larsen, A.H.; Mortensen, J.J.; Blomqvist, J.; Castelli, I.E.; Christensen, R.; Dułak, M.; Friis, J.; Groves, M.N.; Hammer, B.; Hargus, C.; Hermes, E.D.; Jennings, P.C.; Jensen, P.B.; Kermode, J.; Kitchin, J.R.; Kolsbjerg, E.L.; Kubal, J.; Kaasbjerg, K.; Lysgaard, S.; Maronsson, J.B.; Maxson, T.; Olsen, T.; Pastewka, L.; Peterson, A.; Rostgaard, C.; Schiøtz, J.; Schütt, O.; Strange, M.; Thygesen, K.S.; Vegge, T.; Vilhelmsen, L.; Walter, M.; Zeng, Z.; Jacobsen, K.W. The atomic simulation environment-a Python library for working with atoms. *Journal of Physics: Condensed Matter* **2017**; 29, 273002.

[59] Perdew, J.P.; Burke, K.; Ernzerhof, M. Generalized gradient approximation made simple. *Physical Review Letters* **1996**; 77, 3865–3868.

[60] Grimme, S.; Antony, J.; Ehrlich, S.; Krieg, H. A consistent and accurate ab initio parametrization of density functional dispersion correction (DFT-D) for the 94 elements H-Pu. *Journal of Chemical Physics* **2010**; 132.

[61] Axilrod, B.M.; Teller, E. Interaction of the van der Waals type between three atoms. *The Journal of Chemical Physics* **1943**; 11, 299–300.

[62] Muto, Y. On the forces acting between non-polar molecules. *Proceedings of the Physico-Mathematical Society of Japan* **1943**; , 629.

[63] Kittel, C. *Introduction to Solid State Physics*. Wiley, Hoboken, NJ, 8th ed. edition **2005**. ISBN 0471680575.

[64] Lindgren, P.; Kastlunger, G.; Peterson, A.A. Scaled and Dynamic Optimizations of Nudged Elastic Bands. *Journal of Chemical Theory and Computation* **2019**; 15, 5787–5793.

[65] Henkelman, G.; Uberuaga, B.P.; Jónsson, H. Climbing image nudged elastic band method for finding saddle points and minimum energy paths. *Journal of Chemical Physics* **2000**; 113, 9901–9904.

[66] Henkelman, G.; Jónsson, H. Improved tangent estimate in the nudged elastic band method for finding minimum energy paths and saddle points. *Journal of Chemical Physics* **2000**; 113, 9978–9985.

[67] Kresse, G.; Furthmüller, J. Efficiency of Ab-Initio Total Energy Calculations for Metals and Semiconductors Using a Plane-Wave Basis Set. *Computational Materials Science* **1996**; 6, 15–50.

[68] Kresse, G.; Furthmüller, J. Efficient Iterative Schemes for *Ab Initio* Total-Energy Calculations Using a Plane-Wave Basis Set. *Physical Review B* **1996**; 54, 11169–11186.

[69] Wellendorff, J.; Lundgaard, K.T.; Møgelhøj, A.; Petzold, V.; Landis, D.D.; Nørskov, J.K.; Bligaard, T.; Jacobsen, K.W. Density Functionals for Surface Science: Exchange-correlation Model Development with Bayesian Error Estimation. *Physical Review B* **2012**; 85, 235149.

[70] Frederiksen, T.; Paulsson, M.; Brandbyge, M.; Jauho, A.P. Inelastic transport theory from first principles: Methodology and application to nanoscale devices. *Physical Review B - Condensed Matter and Materials Physics* **2007**; 75, 1–22.

[71] Farahvash, A.; Agrawal, M.; Peterson, A.A.; Willard, A.P. Modeling Surface Vibrations and Their Role in Molecular Adsorption: A Generalized Langevin Approach. *J. Chem. Theory Comput.* **2023**; 19, 6452–6460.

[72] Sprowl, L.H.; Campbell, C.T.; Árnadóttir, L. Hindered translator and hindered rotor models for adsorbates: Partition functions and entropies. *Journal of Physical Chemistry C* **2016**; 120, 9719–9731.

[73] Blöndal, K.; Sargsyan, K.; Bross, D.H.; Ruscic, B.; Goldsmith, C.F. Adsorbate Partition Functions via Phase Space Integration: Quantifying the Effect of Translational Anharmonicity on Thermodynamic Properties. *Journal of Physical Chemistry C* **2021**; 125, 20249–20260.

[74] Blöndal, K.; Sargsyan, K.; Bross, D.H.; Ruscic, B.; Goldsmith, C.F. Configuration Space Integration for Adsorbate Partition Functions: The Effect of Anharmonicity on the Thermophysical Properties of CO–Pt(111) and CH_3OH–Cu(111). *ACS Catal.* **2023**; 13, 19–32.

[75] Blöndal, K.; Badger, K.; Sargsyan, K.; Bross, D.H.; Ruscic, B.; Goldsmith, C.F. Importance Sampling within Configuration Space Integration for Adsorbate Thermophysical Properties: A Case Study for CH_3 /Ni(111). *Physical Chemistry Chemical Physics* **2024**; 26, 17265–17273.

[76] Feibelman, P.J.; Hammer, B.; Nørskov, J.K.; Wagner, F.; Scheffler, M.; Stumpf, R.; Watwe, R.; Dumesic, J. The CO/Pt(111) Puzzle. *The Journal of Physical Chemistry B* **2001**; 105, 4018–4025.

[77] Peterson, A.A. Global optimization of adsorbate-surface structures while preserving molecular identity. *Topics in Catalysis* **2014**; 57, 40–53.

[78] Goedecker, S. Minima hopping: An efficient search method for the global minimum of the potential energy surface of complex molecular systems. *The Journal of Chemical Physics* **2004**; 120, 9911–9917.

[79] Zhang, Y.J.; Sethuraman, V.; Michalsky, R.; Peterson, A.A. Competition between CO_2 Reduction and H_2 Evolution on Transition-Metal Electrocatalysts. *ACS Catalysis* **2014**; 4, 3742–3748.

[80] Blondal, K.; Jelic, J.; Mazeau, E.; Studt, F.; West, R.H.; Goldsmith, C.F. Computer-Generated Kinetics for Coupled Heterogeneous/Homogeneous Systems: A Case Study in Catalytic Combustion of Methane on Platinum. *Industrial and Engineering Chemistry Research* **2019**; 58, 17682–17691.

[81] Kreitz, B.; Gusmão, G.S.; Nai, D.; Sahoo, S.J.; Peterson, A.A.; Bross, D.H.; Goldsmith, C.F.; Medford, A.J. Unifying thermochemistry concepts in computational heterogeneous catalysis. ChemRxiv **2024**. (accessed 2024-09-05).

[82] Miller, S.; Dsilva, C.; Kitchin, J.R. Coverage dependent adsorption properties of atomic adsorbates on late transition metal surfaces. In *Catalysis: Volume 24*, volume 24. The Royal Society of Chemistry. ISBN 978-1-84973-375-5 **2012**; pp. 83–115.

[83] Kreitz, B.; Lott, P.; Studt, F.; Medford, A.J.; Deutschmann, O.; Goldsmith, C.F. Automated Generation of Microkinetics for Heterogeneously Catalyzed Reactions Considering Correlated Uncertainties. *Angewandte Chemie International Edition* **2023**; 62, e202306514.

[84] Kreitz, B.; Blöndal, K.; Badger, K.; West, R.H.; Goldsmith, C.F. Automatic Mechanism Generation Involving Kinetics of Surface Reactions with Bidentate Adsorbates. *Digital Discovery* **2024**; 3, 173–185.

[85] Kreitz, B.; Wehinger, G.D.; Goldsmith, C.F.; Turek, T. Microkinetic Modeling of the CO_2 Desorption from Supported Multifaceted Ni Catalysts. *The Journal of Physical Chemistry C* **2021**; 125, 2984–3000.

[86] Iyer, G.R.; Rubenstein, B.M. Finite-Size Error Cancellation in Diffusion Monte Carlo Calculations of Surface Chemistry. *The Journal of Physical Chemistry A* **2022**; 126, 4636–4646.

[87] Gunasooriya, G.K.K.; Van Bavel, A.P.; Kuipers, H.P.; Saeys, M. CO Adsorption on Cobalt: Prediction of Stable Surface Phases. *Surface Science* **2015**; 642, L6–L10.

[88] Papp, H. The Chemisorption of Carbon Monoxide on a Co(0001) Single Crystal Surface; Studied by LEED, UPS, EELS, AES and Work Function Measurements. *Surface Science* **1983**; 129, 205–218.

[89] Lahtinen, J.; Vaari, J.; Kauraala, K. Adsorption and Structure Dependent Desorption of CO on Co(0001). *Surface Science* **1998**; 418, 502–510.

[90] Lansford, J.L.; Mironenko, A.V.; Vlachos, D.G. Scaling relationships and theory for vibrational frequencies of adsorbates on transition metal surfaces. *Nature Communications* **2017**; 8.

[91] Hill, T.L. *An Introduction to Statistical Thermodynamics*. Dover, New York **1960**.

[92] Cardona-Martinez, N.; Dumesic, J.A. Applications of Adsorption Microcalorimetry to the Study of Heterogeneous Catalysis. *Advances in Catalysis* **1992**; 38, 149–244.

[93] Adamson, A.; Gast, A. *Physical chemistry of surfaces*. Wiley, New York, 6th edition **1997**. ISBN 978-0-471-14873-9.

[94] Savara, A. Standard states for adsorption on solid surfaces: 2D gases, surface liquids, and Langmuir adsorbates. *Journal of Physical Chemistry C* **2013**; 117, 15710–15715.

[95] Shell, M.S. Solutions: advanced and special cases. In *Thermodynamics and Statistical Mechanics*. Cambridge University Press, Cambridge **2015**; pp. 217–220.

[96] Ward, B.M.; Getman, R.B. Molecular simulations of physical and chemical adsorption under gas and liquid environments using force field- and quantum mechanics-based methods. *Molecular Simulation* **2014**; 40, 678–689.

[97] Rommens, K.T.; Gunasooriya, G.K.K.; Saeys, M. Key Role of CO Coverage for Chain Growth in Co-Based Fischer–Tropsch Synthesis. *ACS Catalysis* **2024**; 14, 6696–6709.

[98] Lin, X.; Hass, K.C.; Schneider, W.F.; Trout, B.L. Chemistry of sulfur oxides on transition metals I: Configurations, energetics, orbital analyses, and surface coverage effects of SO2 on Pt(111). *Journal of Physical Chemistry B* **2002**; 106, 12575–12583.

[99] Yang, N.; Medford, A.J.; Liu, X.; Studt, F.; Bligaard, T.; Bent, S.F.; Nørskov, J.K. Intrinsic Selectivity and Structure Sensitivity of Rhodium Catalysts for C $_{2+}$ Oxygenate Production. *Journal of the American Chemical Society* **2016**; 138, 3705–3714.